STABILITY ANALYSIS WITH NON-RIGID WEDGES

C. Santamarina[1] and G.A. Leonards[2]

SUMMARY. Current limiting equilibrium analyses of the stability of slopes assume rigid wedges. A new approach that relaxes this requirement is proposed in this paper. The calculation algorithm and a computer program based on it are described. It is shown that the stiffness of the wedge and the interaction along the sliding surface are important factors affecting the stability of slopes.

1. Introduction

Conventional slope stability analyses assume rigid wedges, hence the relation between the shear stress mobilized along the slip surface and the deformation of the soil mass is not considered. While these algorithms have proved useful in examining the safety of slopes in limiting equilibrium, they do not favor understanding the fundamental nature of slope stability. Indeed, the sliding wedge interacts with the base material: the associated modification of internal forces produces deformations within the sliding wedge (and within the base material); these deformations and the stiffness of the wedge mobilize varying fractions of the resistance along the base of the slide. The wedge-base interaction determines the stability conditions of the slope.

Some phenomena cannot be adequately studied unless the nature of this interaction is modeled. Examples include the development of progressive failure in strain-softening soils, and the use of anchors or other synthetic inclusions to improve stability. This paper presents an attempt to model the interaction process by relaxing the rigidity requirement. In this first attempt a number of simplifying assumptions are made in order to highlight the basic concepts.

2. Formulation and Algorithm

The solution presented herein assumes that interslice forces are parallel to the sliding plane, and that slices translate without rotation. The force mobilized at the base of the slice is taken as a function of the displacement parallel to the sliding plane $\delta_i^{//}$

$$T_{mob} = \alpha\ T_{max} \qquad \text{where } \alpha = f(\delta_i^{//}) \text{ and } T_{max} = \text{shear strength} \qquad (1)$$

Utilizing the Mohr-Coulomb failure criterion,

$$T_{mob} = \alpha\ N_i\ \tan\phi_i + \alpha\ c_i \frac{b}{\cos\beta_{ave}} \qquad (2)$$

---

1. Assistant Professor, Polytechnic University, Brooklyn, NY

2. Professor, Purdue University, West Lafayette, IN

where N_i is the effective normal force, b is the slice thickness and β_{ave} is the average slope at the base of the slice (see Figure 1). The two force equilibrium equations for slice "i" are:

$$\Sigma F_x = 0 = f_i \cos\beta_i - f_{i+1}\cos\beta_{i+1} - T_{mob}\cos\beta_{ave} + N_i \sin\beta_{ave} \quad (3)$$

$$\Sigma F_y = 0 = f_i \sin\beta_i - f_{i+1}\sin\beta_{i+1} - T_{mob}\sin\beta_{ave} - N_i \cos\beta_{ave} + W_i \quad (4)$$

Introducing equation 2 in 3&4, and solving for N_i,

$$N_i = \frac{f_i \sin(\beta_{i+1}-\beta_i) - \frac{\alpha c_i b}{\cos\beta_{ave}} \sin(\beta_{i+1}-\beta_{ave}) - W_i \cos\beta_{i+1}}{\alpha \tan\phi_i \sin(\beta_{i+1}-\beta_{ave}) - \cos(\beta_{ave}-\beta_{i+1})} \quad (5)$$

And from equation 3

$$f_{i+1} = \frac{f_i \cos\beta_i - T_{mob}\cos\beta_{ave} + N_i \sin\beta_{ave}}{\cos\beta_{i+1}} \quad (6)$$

The horizontal deformation of a given slice is calculated using the change in the horizontal components of the interslice forces due to excavation. The displaced position of the interslice plane "i+1" is obtained by adding the width "b" to the displaced position of the interslice plane "i", and the change in width Δb of the i^{th} slice. Δb results from the change in the average interslice forces between the initial values and the current ones:

$$x_{i+1} = x_i + b + \frac{(\Delta f_i \cos\beta_i + \Delta f_{i+1}\cos\beta_{i+1})}{2} \frac{b}{E_i h_i} \quad (7)$$

where E_i is Young's modulus for the material in the i^{th} slice, and h_i is the height of the slice. Then, the displacement parallel to the sliding plane for the <u>next</u> slice can be computed as follows,

$$\delta_i'' = \frac{(x_i^0 - x_i^{new}) + (x_{i+1}^0 - x_{i+1}^{previous})}{2 \cos\beta_{ave}} \quad (8)$$

The calculation algorithm is summarized in Table 1.

Known:	f_1 and f_{n+1}	
Assume:	x_i^{new} for i=1	
Calculate:	δ_i''	(equation 8)
	α	(predefined function of δ_i'')
	N_i	(equation 5)
	T_{mob}	(equation 2)
	f_{i+1}	(equation 6)
	x_{i+1}^{new}	(equation 7)
Check equilibrium at toe:		
	IF $f_{n+1}^{calc} > f_{n+1}^{known}$ THEN increase x_1^{new}	

Table 1: Calculation Algorithm

3. Initial Forces

Similar to other analyses where the effects of deformations are accounted for, the initial interslice forces must be known. In the case of level ground, prior to an excavation, the geostatic in situ state of stress results in initial interslice forces normal to the vertical slices. During excavation there is a rotation of principal stresses. Herein, it is assumed that the directions of the interslice forces are parallel to the slope surface and that only the normal components of the interslice forces cause dimensional changes in the width of the slices.

The at-rest condition also involves shear stresses on inclined planes. On the preselected sliding surface

$$\tau_0 = \sigma_1(1-k_0)\ \sin(\beta_{ave}) \tag{9}$$

Hence, there is an associated initial value T_0, and equation 1 is modified as follows,

$$T_{mob} = T_0 + \alpha\ T_{max} \tag{10}$$

4. Modulus Degradation and Tension Cracks

It is known that Young's modulus decreases with the increase in stress ratio σ_1/σ_3 and strain level ϵ, and with the decrease in confining stresses σ_c. These three parameters are affected when a slope is activated. In fact, during lateral unloading such as in the excavation of level ground, the three parameters are affected in a sense that reduces E.

This effect can be modeled. For example, a rule can be used to vary the modulus of each slice as a function of the interslice forces, from an initial value E_{high-i} to a final value $E_{low-i} = \rho E_{high-i}$. Assuming a simple liner model,

$$E_i = E_{high-i} * \left[\frac{f_i+f_{i+1}}{f_i^0+f_{i+1}^0}\ (1 - \rho) + \rho\right] \tag{11}$$

E_{low} in granular materials becomes eventually zero when there is no confinement, and a tension crack does not develop. On the other hand, $E_{low}>0$ in unconfined saturated fine grained soils that where unloaded in undrained conditions; a tension crack may develop within the slope, splitting the wedge into a stationary and a moving mass.

5. Computer Program

A computer program was developed using the algorithm and concepts discussed above. The slide is represented by n slices of equal width. Each slice and each interslice plane have an associated list of attributes, shown in Figure 1.

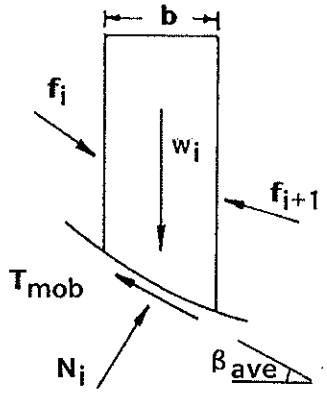

Slice

w(i)	weight
h(i)	height
E(i)	Young's Modulus
s(i)	Shear Strength
ϕ(i)	Friction Angle
δ(i)	Deformation to Yield

Interslice Plane

f_i^0 & f_{i+1}^0	Initial Interslice Forces
f_i & f_{i+1}	Calculated Interslice Forces
x_i	Position of interslice plane i

Figure 1: A Slice and Its Attributes

An elasto-plastic model for the shear stress along the sliding surface has been implemented in the current version. If T_{mob} is normalized with respect to T_{max}, the soil model is represented by the α function (Equations 1 and 10) as shown in Figure 2. A strain softening condition (dashed line in Figure 2) can readily be implemented

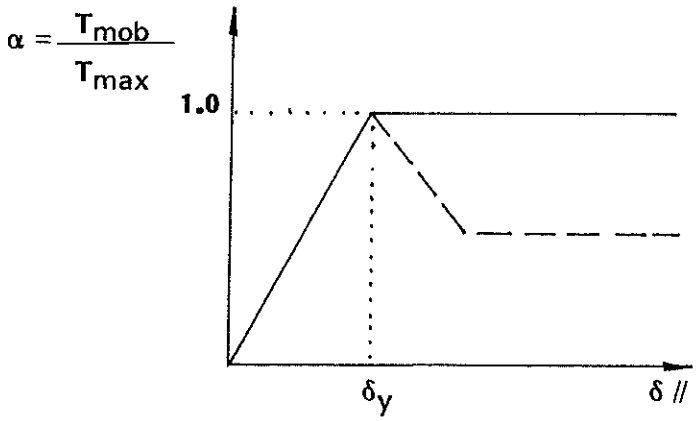

Figure 2: Soil Model at the Base of the Slices

There are very limited field data to guide the estimation of δ_y. However, δ_y must be related to the shear modulus and the thickness t of the shear zone.

$$G = \frac{E_u}{2(1+\nu)} \sim \frac{\tau_{max}}{\delta_y/t} \qquad (12)$$

For the case of undrained loading, Poisson's ratio is $\nu = 0.5$ and assuming a reasonable relation between $E_{u\text{-}ave} = 200$ to 600 S_u, the estimate for δ_y is between t/50 to t/150. The thickness of the shear zone, t, may range from a few centimeters to a meter or more.

Because the position of the slices changes as the wedge deforms and the shear strength is mobilized, β_i's are reevaluated in every iteration. To facilitate this calculation, the sliding plane is defined as a curve with continuous first derivative. Two functions are included in the current version: fourth degree polynomial curve and circular arc.

The user may input the initial values of the interslice forces and shear forces at the base of the slices, or run an option that generates them automatically, assuming at-rest conditions for the unexcavated slope.

The program outputs the local factor of safety, $FS_L = T_{max(i)}/T_{mob(i)}$, the interslice forces, the displaced position of each slice, and the total strain energy. A global factor of safety is also computed for circular failure surfaces, based on moment equilibrium of the entire wedge,

$$FS_{Global} = \frac{\Sigma\ T_{max}}{\Sigma\ T_{mob}} \qquad (13)$$

In each run, the output indicates any negative interslice forces. A limiting tensile strength can also be specified; in this case the program outputs the negative interslice forces that exceed this limit. The formation of a tension crack can be simulated by fixing the interslice force equal to zero and re-running the program.

6. Sample Runs

The following examples study illustrate the proposed method of analysis, and shows the influence of the stiffness of the wedge material (E) and the deformation needed to mobilize the shear strength along the failure plane (δ_y) on the behavior of the slope. The case modeled is that of level ground that is subsequently excavated vertically to a depth of 10 m. A clay soil was selected, with total unit weight $\gamma_{tot} = 2000$ kg/m^3, and undrained shear strength $s_u = 1.0$ kg/cm^2. These parameters result in stability numbers $s_u/\gamma H$ of 0.250 for Cullmann's method, and 0.261 for solutions based on circular and logarithmic spiral failure surfaces.

The critical circular failure surface was selected using the Simplified Bishop's Method, then the current program was run. For the calculation of the initial forces, an isotropic state of stresses was assumed, $k_0 = 1.0$, therefore $T_0 = 0$. Two levels of undrained modulus were selected for the parametric study: $E_u = 200 s_u = 200$ kg/cm^2, and $E_u = 600 s_u = 600$ kg/cm^2. Three levels of deformation to yield the shear strength along the sliding plane were used: $\delta_y = 0.06$cm, 0.2cm, and 1.0cm. The linear modulus degradation function suggested in Equation 11 was used, with $\rho = 0.1$.

Table 2 summarizes the results obtained. Depending on the modulus and the deformation to yield, tensile interslice forces can develop. In those cases ($E_u = 600$kg/cm^2 and $\delta_y = 0.2$ and 1.0), an arbitrary tensile interslice force of up to $0.1 S_u h_i$ was allowed. The negative interslice forces did not exceed this bound in any case, hence no tensile crack was modeled. The interslice forces shown in Figure 3. Figure 4 shows the local factor of safety in each case.

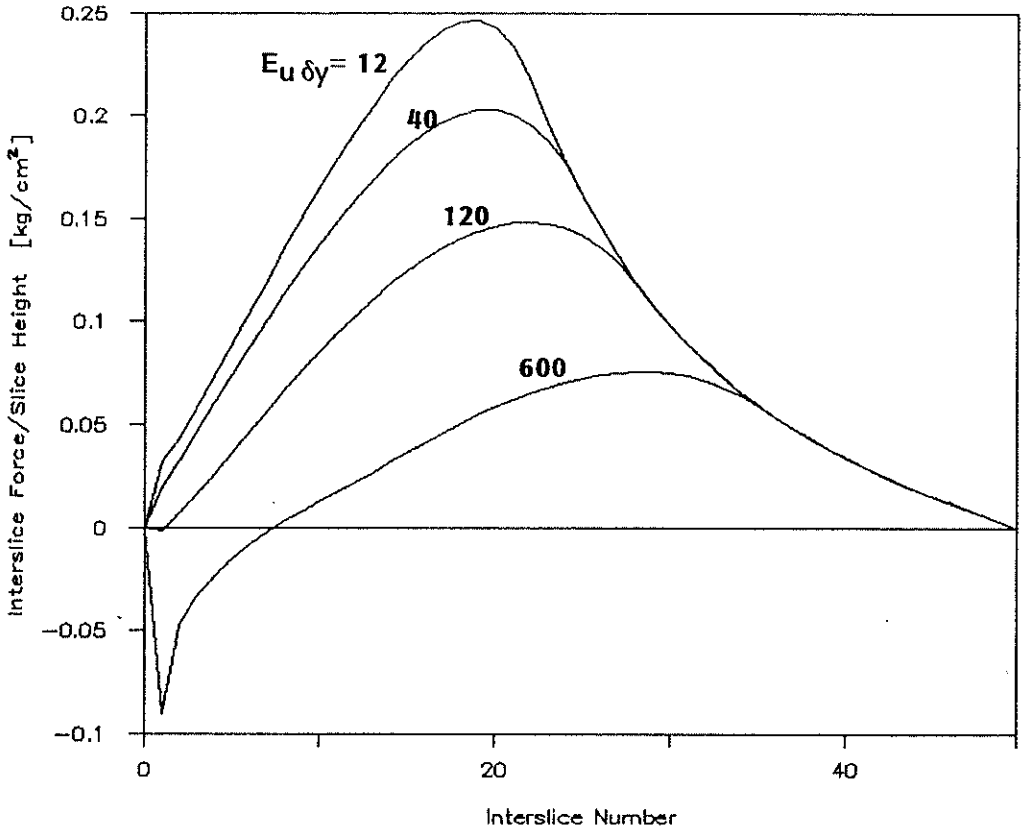

Figure 3: Interslice Forces

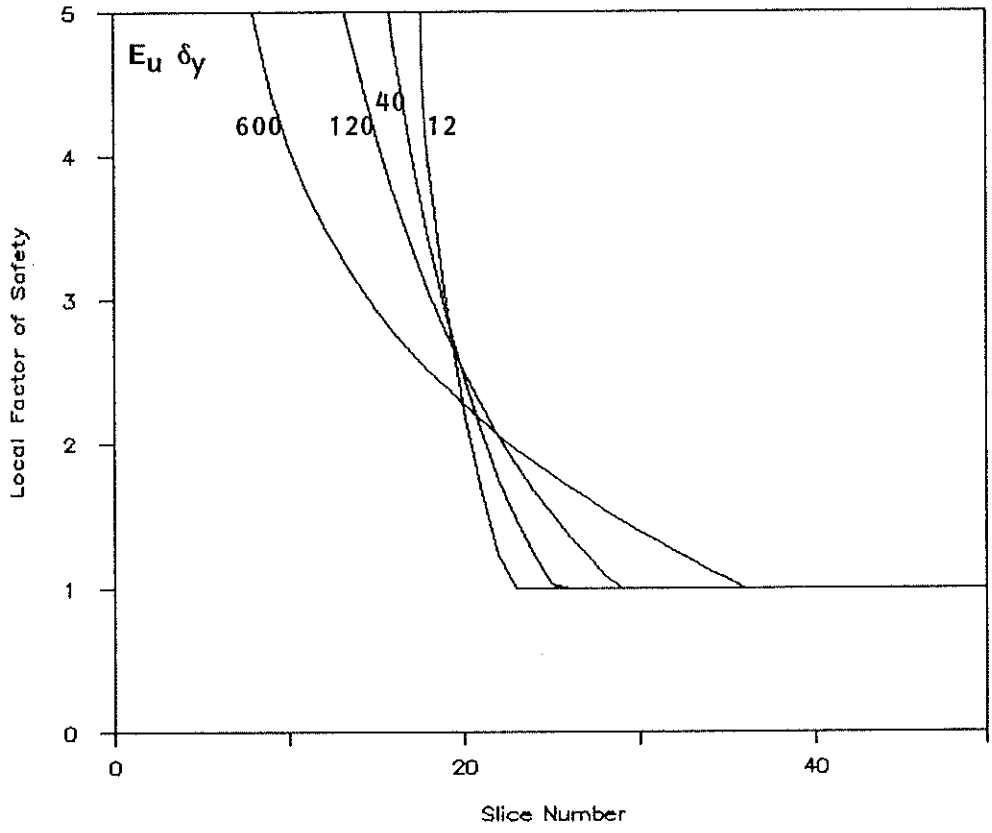

Figure 4: Local Factor of Safety

Non-Rigid Analysis

E_u	δ_y	$E_u*\delta_y$	t [cm]	FS_{Global}	Notes
200	0.06	12	4	1.922	no-tension
200	0.2	40	13	1.922	no-tension
600	0.2	120	40	1.921	tension, no-crack
600	1.0	600	200	1.921	tension, no-crack

Rigid Wedge Analysis

Method	FS_{Global}
Closed Form Solutions	1.916[2]
Bishop's Simp. Meth.	1.923[3]
Janbu's Method	2.059

Notes
1: Tensile stresses up to 0.1 Su were allowed between slices
2: Based on circular or log spiral surfaces.
3: Tension in the top 12 interslices out of 50 slices

Table 2: Parametric Study - Results

Based on the results presented here, and others not shown, the following observations can be made:

- The product $E_u*\delta_y$ appears to be very important in characterizing the interaction between the sliding mass and the base material. As shown in Equation 12, it represents the thickness of the shear zone times the shear strength.
- For a given wedge stiffness, the pattern of displacements is similar for different δ_y. The lateral expansion of the wedge as a result of lateral unloading is clearly shown.
- The lower $E_u*\delta_y$, the higher the interslice forces.
- The distribution of the interslice forces is quite sensitive to assumptions regarding modulus degradation, allowable tensile interslice forces and crack formation.
- While the global factor of safety is the same, the distribution of the local factor of safety is very sensitive to $E_u*\delta_y$.
- For a given geometry, failure tends to start at the bottom of the slide for low $E_u*\delta_y$, and at the crest for high $E_u*\delta_y$.

The last observation is based on the distribution of the local factors of safety (Figure 4), and was confirmed with other cases not presented in this paper.

Finally, the effect of the initial state of stress was analyzed changing the value of K_0 in the generation of the initial forces for the case of E_u= 600 kg/cm^2 and δ_y= 0.2cm. The value of K_0 was varied from 0.2 to 1.4, and a modulus degradation ratio ρ= 0.1 was used. The global factors of safety

were identical in all cases (FS_{global}= 1.921). Figure 5 shows the effect of K_0 on the local factors of safety.

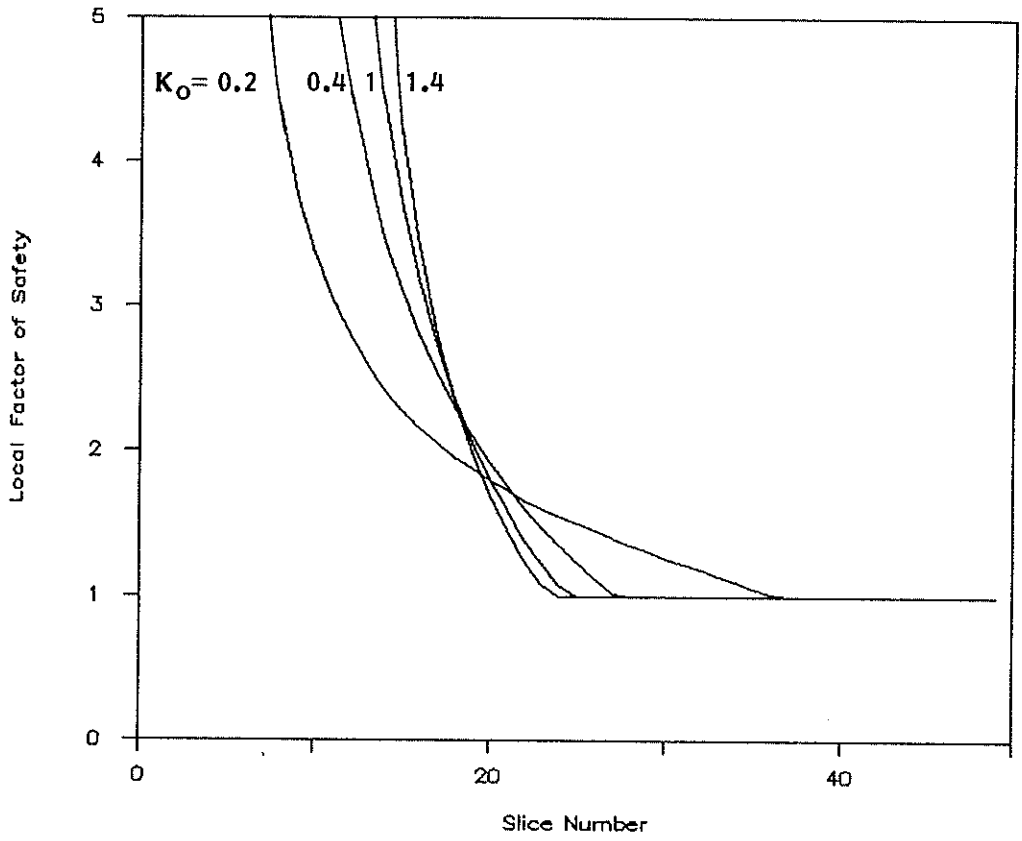

Figure 5: Local Factor of Safety - Effect of K_0

7. Conclusions

A new algorithm for the stability analysis of slopes was introduced. Its salient characteristic is the relaxation of the rigidity requirement. It was shown that the stiffness of the sliding material and the deformation needed to mobilize the shear strength along the sliding surface are very important parameters affecting the behavior of earth slopes.